Structural Changes in the O-Decay Accelerated Mutants of *pharaonis* Phoborhodopsin†

Yuki Sudo,‡,⊥ Yuji Furutani,‡ Masayuki Iwamoto,§ Naoki Kamo,|| and Hideki Kandori*,‡

Department of Materials Science and Engineering, Nagoya Institute of Technology, Showa-ku, Nagoya 466-8555, Japan, Division of Molecular Physiology and Biophysics, Department of Morphological and Functional Biomedical Science, Faculty of Medical Science, University of Fukui, Matsuoka 910-1193, Japan, and Laboratory of Biophysical Chemistry, Graduate School of Pharmaceutical Sciences, Hokkaido University, Sapporo 060-0812, Japan

Received September 14, 2007; Revised Manuscript Received December 10, 2007

ABSTRACT: *pharaonis* phoborhodopsin (*p*pR, also called *pharaonis* sensory rhodopsin II, *p*sRII) is a receptor for negative phototaxis in *Natronomonas pharaonis*. The X-ray crystallographic structure of *p*pR is very similar to those of the ion-pumping rhodopsins, bacteriorhodopsin (BR) and halorhodopsin (hR). However, the decay processes of the photocycle intermediates such as M and O are much slower than those of BR and hR, which is advantageous for the sensor function of *p*pR. Iwamoto et al. previously found that, in a quadruple mutant (P182S/P183E/V194T/T204C; denoted as SETC) of *p*pR, the decay of the O intermediate was accelerated by ~100 times ($t_{1/2}$ ~6.6 ms vs 690 ms for the wild type of *p*pR), being almost equal to that of BR (Iwamoto, M., et al. (2005) *Biophys. J. 88*, 1215–1223). The mutated residues are located on the extracellular surface (Pro182, Pro183, and Val194) and near the Schiff base (Thr204). The present Fourier-transform infrared (FTIR) spectroscopy of SETC revealed that protein structural changes in the K and M states were similar to those of the wild type. In contrast, the *p*pR_O minus *p*pR infrared difference spectra of SETC are clearly different from those of the wild type in amide-I (1680–1640 cm^{-1}) and S−H stretching (2580–2520 cm^{-1}) vibrations. The 1673 (+) and 1656 (−) cm^{-1} bands newly appear for SETC in the frequency region typical for the amide-I vibration of the α_{II}- and α_I-helices, respectively. The intensities of the 1673 (+) cm^{-1} band of various mutants were well correlated with their O-decay half-times. Since the α_{II}-helix possesses a considerably distorted structure, the result implies that distortion of the helix is required for fast O-decay. In addition, the characteristic changes in the S−H stretching vibration of Cys204 were different between SETC and T204C, suggesting that structural change near the Schiff base was induced by mutations of the extracellular surface. We conclude that the lifetime of the O intermediate in *p*pR is regulated by the distorted α-helix and strengthened hydrogen bond of Cys204.

pharaonis phoborhodopsin, *p*pR[1] (also called *pharaonis* sensory rhodopsin II, *p*sRII), from *Natronomonas* (*Natronobacterium*) *pharaonis*, is a seven-transmembrane helical protein into which a chromophore, all-*trans* retinal, binds to a specific lysine residue (Lys205) on the G-helix to form a protonated Schiff base (*1–3*). A carboxylic acid, Asp75, serves as one of two counterions of the protonated Schiff base (Figure 1) (*4, 5*). These structural features are essentially common among other archaeal rhodopsins such as bacteriorhodopsin (BR) (*6, 7*), halorhodopsin (hR) (*8*), and sensory rhodopsin (sR or SRI) (*9*), which function as an outward light-driven proton pump, inward light-driven Cl^- pump, and phototaxis sensor other than for phoborhodopsin, respectively (*9*). *p*pR forms a signaling complex with *pharaonis* halobacterial transducer protein, *p*HtrII, in the membrane and transmits light signals to the *p*HtrII through the changes in such an interaction (*2, 3*). *p*HtrII activates phosphorylation cascades that modulate flagella motors. Consequently, these bacteria avoid short wavelength light (λ < 520 nm), which contains harmful near-UV rays. The function is called negative phototaxis (*9*).

*p*pR is highly stable within the membrane and detergent micelles as well as *p*HtrII (*10*), and a functional expression system utilizing *E. coli* cells can provide large amount of proteins (*11, 12*). Therefore, *p*pR and *p*HtrII have been well characterized over the past several years using various methods (*1–3*). The crystallographic structure of *p*pR and the *p*pR/*p*HtrII complex had been achieved (*13–15*), and light-induced structural changes were also identified by

† This work was supported by grants from Japanese Ministry of Education, Culture, Sports, Science, and Technology to H.K. (15076202).

* To whom correspondence should be addressed. Phone and Fax: 81-52-735-5207 . E-mail: kandori@nitech.ac.jp.

‡ Nagoya Institute of Technology.

§ University of Fukui.

|| Hokkaido University.

⊥ Present address: Division of Biological Science, Graduate School of Science, Nagoya University, Chikusa-Ku, Nagoya, 464-8602, Japan.

[1] Abbreviations: *p*pR, *pharaonis* phoborhodopsin; FTIR, Fourier-transform infrared; *p*pR_K, K intermediate of *p*pR; *p*pR_M, M intermediate of *p*pR; *p*pR_O, O intermediate of *p*pR; SET, a *p*pR triple mutant, P182S/P183E/V194T; SETC, a *p*pR quadruple mutant, P182S/P183E/V194T/T204C; P183E and T204C, *p*pR mutants in which Pro183 or Thr204 are substituted by Glu and Cys, respectively; BR, light-adapted bacteriorhodopsin that has all-*trans* retinal as its chromophore; PRG, proton releasing group; EC, exctracellular proton conduction channel.

10.1021/bi701885k CCC: $40.75
Published on Web 02/05/2008

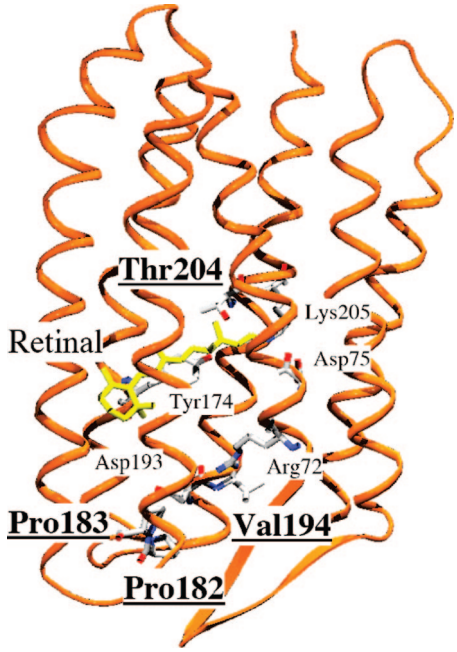

FIGURE 1: X-ray crystallographic structure of *p*pR. The amino acid residues that were replaced in the present study are underlined, while other important residues are also indicated. It is suggested that Thr204 forms a hydrogen bond with Tyr174. Upper and lower regions correspond to the cytoplasmic and extracellular sides, respectively. This structure was obtained from the Protein Data Bank (code 1H68) (*14*).

various methods, including UV–vis, electron paramagnetic resonance (EPR) spectroscopy, and so forth (*1–3*). Interestingly, the structure and structural changes are almost the same as those of BR (*16*) and hR (*8*), implying that the functional differentiation was caused by small structural differences in some amino acid side chain(s) and/or main chain(s). In fact, we recently reported that substitution of only three residues, P200T/V210Y/A215T, converted BR into a negative phototosensor such as *p*pR (SRII), indicating similar structural changes between BR and *p*pR (SRII) (*17*). We further analyzed the early intermediates of the mutant by Fourier-transform infrared (FTIR) spectroscopy and found that the structural changes of the α helix and Thr215 corresponding to Thr204 of *p*pR (*p*SRII) are similar to those of *p*pR (*p*SRII) (*18*).

The chromophore of *p*pR is photoexcited by blue light, and the protein undergoes a thermal linear reaction cycle, the photocycle, through some intermediates accompanying the conformational change of the protein (*19*). The intermediates of *p*pR are denoted as K, L, M, N, and O, analogous to those of BR (*20*). The active (signaling) intermediates of the *p*pR are referred to as the M and O intermediates (*21*). Interestingly, the decay rates of these intermediates are much slower than those of BR and the O intermediate of hR (*20*), despite the similarity in their X-ray crystallographic structures (*13–15*). Upon BR_M formation in the BR photocycle, primary proton transfer takes place from the protonated Schiff base to its counterion, Asp85 (*22*). The following cascade of proton movements, such as uptake from the intracellular side and the transfer from Asp96 to the deprotonated Schiff base, results in the proton pumping of BR from the cytoplasmic to the extracellular side (*23*). *p*pR also exhibits a light-driven proton pumping activity like that of BR, although the activity is very weak (*24, 25*). Comparing the primary sequence of BR and *p*pR, it becomes evident that a change of an amino acid(s) in the cytoplasmic channel might be responsible for these differences because Asp96 and Thr46 have been reported to be crucial for the proton pumping mechanism of BR (*26, 27*). In *p*pR, Asp96 is replaced by a neutral residue, Phe86. Thr46, which is involved in tuning the pK_a of Asp96 in BR, is also missing. Iwamoto et al. previously reported that the M-decay of this replacement mutant (L40T/F86D) was highly accelerated from 890 ms for the wild type to about 5 ms (∼180 times) (*28*), being almost equal to that for BR. These mutated residues were located on the cytoplasmic side, implying that M-decay was controlled by a cytoplasmic channel (*28*). Thereafter, Iwamoto et al. studied protein structural changes and the proton transfer reaction during the photocycle of the F86D mutant of *p*pR in detail by means of FTIR spectroscopy (*29*). Furthermore, the light-induced F-helix movement on the cytoplasmic side was demonstrated by various groups, and the movement is believed to play an important role in the activation of *p*HtrII (*1, 30*).

How about the kinetics for the O intermediate? In BR, mutations at Glu194 and Glu204, which constitute the proton-releasing group (PRG) on the extracellular channel, led to slow O-decay (*31–35*). A comparison of the amino acid alignment of BR and *p*pR suggests that the extracellular channel of *p*pR is more hydrophobic than that of BR (*36*). We previously reported that the O-decay of this replacement quadruple mutant (P182S/P183E/V194T/T204C) was highly accelerated from 690 ms for the wild type to about 6.6 ms (∼100 times) (*37*), being almost equal to that for BR. However, the precise roles of these residues in the structural change during the photocycle remain unclear.

In order to determine the structural features required for the regulation of O-decay, we analyzed here protein conformational changes during the photocycles of the various O-decay accelerated mutants in *p*pR by using FTIR spectroscopy. FTIR spectroscopy is a powerful tool for investigating protein structure and the structural changes of rhodopsins (*38*). Using this method, light-induced structural changes in the O-decay accelerated mutants were compared with those of the wild type upon the formation of the K, M, and O intermediates. FTIR difference spectra of the K and M intermediates are similar among the various mutants and the wild type (*5, 39*). This result is consistent with previous reports in which the decay rate constants of these mutants were essentially the same as those of the wild type of *p*pR (*37, 40*). In contrast, the ppR_O minus *p*pR infrared difference spectra of the mutants are clearly different from those of the wild type in amide-I (1680–1640 cm^{-1}) and S−H stretching (2580–2520 cm^{-1}) vibrations. The 1673 (+) and 1656 (−) cm^{-1} bands newly appear in the frequency region typical for the amide-I vibration of the α_{II}- and α_I-helices, respectively. The intensities of the 1673 (+) and 1656 (−) cm^{-1} bands of various mutants were well correlated with the decay half-times of ppR_O. Since the α_{II}-helix possesses a considerably distorted structure, the result implies that helix distortion is required for fast O-decay. In addition, characteristic changes in the S−H stretching vibration of Cys204 were observed in the quadruple mutant (P182S/P183E/V194T/T204C, see Figure 1). This suggests that structural change near the Schiff base was induced by mutation of the

extracellular surface. The implications of these observations are discussed.

MATERIALS AND METHODS

Preparation of the ppR Samples. Mutant proteins of *p*pR were prepared as described previously (*37, 41*). Briefly, the *p*pR proteins with a six-histidine tag at the C-terminus were expressed in *E. coli* cells, solubilized with 1.0% *n*-dodecyl β-D-maltoside, and purified with a Ni-NTA column as described previously (*12, 39*). The purified samples were then reconstituted into L-α-phosphatidylcholine (PC) liposomes by removal with Bio-Beads (SM2, Bio-Rad, Hercules, CA), where the molar ratio of added PC was 50 times that of the *p*pR proteins.

FTIR Spectroscopy. Low-temperature FTIR spectroscopy was performed with 2-cm^{-1} resolution as described previously (*5, 29, 39*). The *p*pR samples in PC liposomes were washed three times with a buffer at pH 7.0 (2 mM phosphate) for the measurement of the K and M intermediates or pH 5.0 (2 mM citrate, 5 mM NaCl) for the measurement of the O intermediate. Then a 90 μL aliquot of the sample (0.1−1 mg) was dried on a BaF_2 window with a diameter of 18 mm. After hydration by H_2O, the sample was placed in a cell, which was mounted in an Oxford DN-1704 cryostat equipped in the Bio-Rad FTS-60 spectrometer.

The *p*pR_K minus *p*pR difference spectra were measured at 77 K as follows (*39*). Illumination of the *p*pR film with 450 nm light for 2 min at pH 7.0 and 77 K converted *p*pR to *p*pR_K, and subsequent illumination with >560 nm light forced *p*pR_K to revert to *p*pR as described previously (*39*). The *p*pR_M minus *p*pR difference spectra were measured at 230 K and pH 7.0 as follows (*5*). To convert *p*pR to *p*pR_M, the sample was irradiated with >480 nm light for 2 min: subsequent illumination with UV light changed *p*pR_M back into *p*pR. The difference spectrum was calculated from the spectra constructed with 128 interferograms before and after the illumination. Twenty-four spectra obtained in this way were averaged for the *p*pR_K minus *p*pR and *p*pR_M minus *p*pR spectrum.

Unlike for *p*pR_K and *p*pR_M, it is difficult to obtain the pure *p*pR_O minus *p*pR spectrum. We previously reported the *p*pR_O minus *p*pR spectrum for the sample in the absence of NaCl at 260 K and pH 5, where the contribution of *p*pR_M was estimated by use of UV/visible absorption of *p*pR_M and *p*pR_O and subtracted by the scaled *p*pR_M minus *p*pR spectrum (*40*). Since the O-decay half-times of the wild type and various mutants were estimated in the presence of NaCl (*37*), we examined the optimal conditions of low-temperature FTIR spectroscopy to accumulate *p*pR_O for a sample containing NaCl. We tested various temperatures (220–260 K) and pH (*5–7*) by monitoring the O-specific C−C stretch of retinal at 1179 cm^{-1} (*40*) and established the following conditions. The difference spectra were obtained by subtracting the spectra after illumination from those during illumination for hydrated films prepared at pH 5.0 (5 mM NaCl). A band path filter possessing the transmittance between 350 and 500 nm (*40*) was used, which is advantageous to accumulate *p*pR_O. We measured the spectra of the wild type, P183E, and T204C at 260 K, while the spectra of SETC and SET were smaller at 260 K, presumably because of the shortened lifetimes. Therefore, we measured the *p*pR_O minus *p*pR spectra of SETC and SET at 240 K. It should be noted that the spectra of SETC and SET at 240 K were similar to those at 260 K, although the latter were much noisier. Eight spectra obtained from the 128 interferograms were averaged, and we call the spectra the *p*pR_O minus *p*pR in the present study. Although the *p*pR_O minus *p*pR spectra possibly contain *p*pR_M and the N-like species, their contributions are not serious (see below).

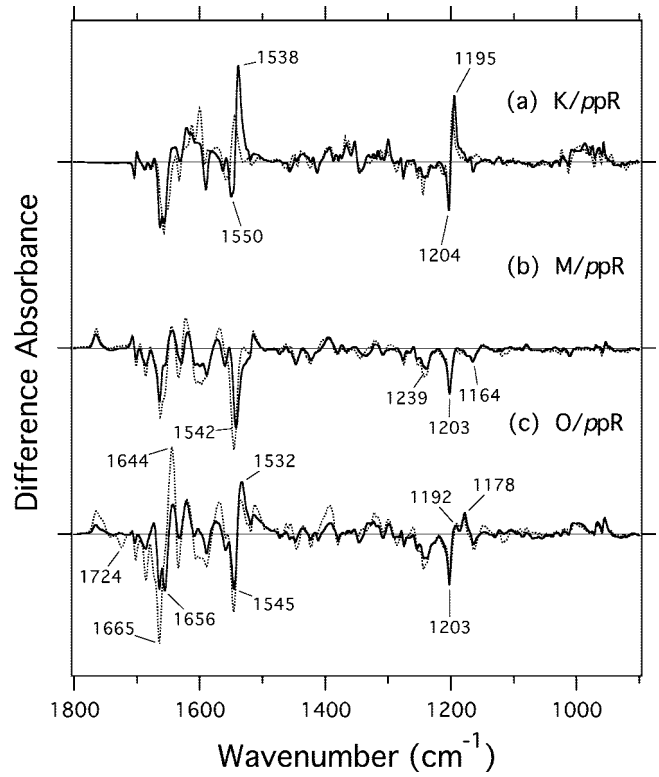

FIGURE 2: *p*pR_K minus *p*pR (a), *p*pR_M minus *p*pR (b), and *p*pR_O minus *p*pR (c) difference FTIR spectra of SETC (—) and the wild type (•••) in the 1800–900 cm^{-1} region. Difference FTIR spectra of the wild type are reproduced from ref *39* for K and ref *5* for M (•••) for comparison. These spectra were measured at 77 K (a) and 230 K (b) for the sample at pH 7. The *p*pR_O minus *p*pR spectra were measured at 260 and 240 K for the wild type and SETC, respectively, at pH 5 (c). One division of the *y*-axis corresponds to 0.016 absorbance units.

RESULTS

Properties of the Mutant Proteins. We first examined the retinal configuration of SETC and other mutant proteins by using HPLC column chromatography (*41*). Consequently, we found that all mutants used in this study (SETC, SET, P183E, and T204C) had only all-*trans* retinal like the wild type (data not shown). This fact suggests that these mutations do not change the structure of the retinal binding pocket. In the UV–vis spectra, SET and P183E showed visible absorption spectra identical to those of the wild type *p*pR (λ_{max} = 498 nm). In contrast, SETC and T204C exhibited red-shifted visible absorption spectra (λ_{max} = 504 nm). This is consistent with previous results in which Thr204 in *p*pR was shown to be one of the important residues for color tuning (*41–43*).

Infrared Spectral Changes of the SETC Mutant of ppR upon the Formation of the K, M, and O Intermediates in the 1800–900 cm^{-1} Region. Figure 2a shows the *p*pR_K minus *p*pR infrared spectrum of SETC measured at 77 K and pH

7.0 (−), which is compared with that of the wild type (•••) (*39*). The vibrational bands at 1550 (−)/1538 (+) cm^{-1} and 1204 (−)/1195 (+) cm^{-1} in SETC correspond to the C═C and C−C stretching vibration of the retinal chromophore, respectively. The lower frequency shift of the former corresponds to the spectral red-shift upon the formation of the K intermediate, while the latter frequency shift represents retinal isomerization from the all-*trans* to the 13-*cis* form (*39*). In addition, similar difference spectra in Figure 2a show that similar structural changes occur in the K formation between SETC and the wild type.

Figure 2b compares the *pp*R_M minus *pp*R infrared spectra of SETC (—) and the wild type (•••) at 230 K and pH 7 (*5*). Similar difference spectra between them also indicate similar structural changes upon the formation of the M intermediate. In the SETC spectrum, the 1542 (−) cm^{-1} band corresponds to the ethylenic C═C stretching mode of the unphotolyzed state. The 1239 (−), 1203 (−), and 1164 (−) cm^{-1} bands are also attributable to the C−C stretching vibrations of the retinal chromophore in the all-*trans* form.

While we can trap *pp*R_K and *pp*R_M under the suitable experimental conditions (temperature and illumination wavelength), that is not the case for *pp*R_O. *pp*R_O is normally observed as a mixture with *pp*R_M and an N-like state. In the previous study, we obtained the *pp*R_O minus *pp*R spectrum after subtracting the contribution of *pp*R_M estimated by using the UV−visible absorption of *pp*R_M and *pp*R_O (*40*). By using 12,14-D_2-labeled retinal, it was clearly shown that *pp*R_O possesses an all-*trans* retinal (*40*). The C−C stretching vibration was observed at 1179 cm^{-1}, which was similar but slightly higher in frequency than that (1168 cm^{-1}) of the O intermediate of BR (*44, 45*). Since the O-decay half-times of the wild type and various mutants were previously estimated in the presence of NaCl (*37*), we newly established the experimental conditions to accumulate *pp*R_O for these proteins. The dotted line in Figure 2c shows the difference spectrum of the wild type, which exhibits the greatest intensity at 1178 cm^{-1}. This suggests that *pp*R_O is optimally accumulated under the present conditions. The ethylenic C═C stretching vibrations at 1545 (−)/1532 (+) cm^{-1} are also characteristic for the O state. It should be noted, however, that this spectrum is considerably different from the *pp*R_O minus *pp*R spectrum in the absence of NaCl (*40*). The difference possibly originates from (i) the effect of NaCl and (ii) the contamination of other intermediates such as *pp*R_M and the N-like species. The present spectrum shows a positive band at 1192 cm^{-1}, characteristic frequency of the protonated 13-*cis* chromophore as seen for *pp*R_K (Figure 2a), which was absent in the previous *pp*R_O minus *pp*R spectrum in the absence of NaCl (*40*). Therefore, it is likely that there is an N-like state containing the protonated 13-*cis*-retinal in the presence of NaCl. From the intensities at 1192 and 1178 cm^{-1}, 20–30% N-like state may be involved as the product. We found that prolonged illumination further intensified the 1192 cm^{-1} band (data not shown), from which characteristic bands of the O-like (1178 cm^{-1}) and N-like (1192 cm^{-1}) species can be separated. It should be noted that the intense peaks at 1665 (−)/1644 (+) cm^{-1} correlate with the 1178 cm^{-1} band, not with the 1192 cm^{-1} band, both characteristic of *pp*R_O. The peaks at 1665 (−)/1644 (+) cm^{-1} do not originate from *pp*R_M because they are absent in the *pp*R_M minus *pp*R spectrum ((•••) in Figure 2b). Thus, in this article, we regard the spectrum ((•••) in Figure 2c) obtained in this way as the *pp*R_O minus *pp*R.

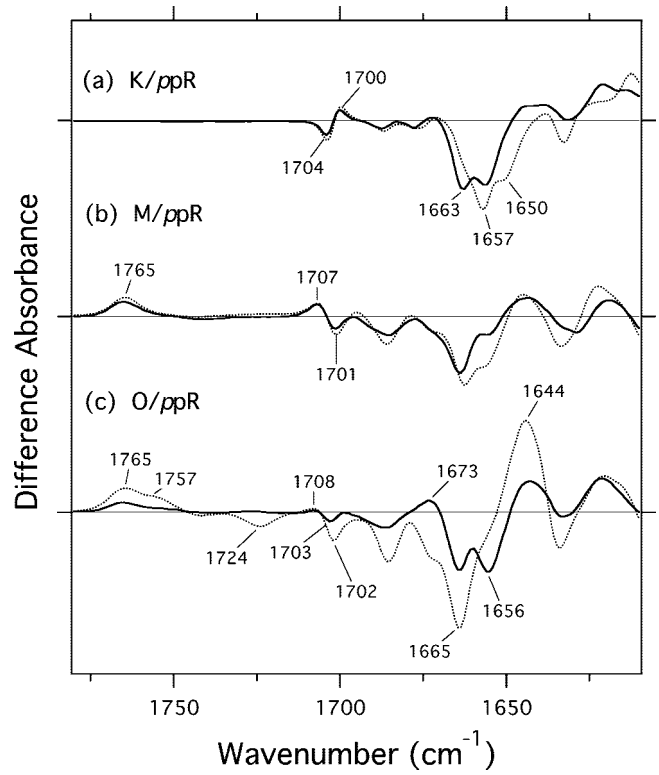

FIGURE 3: *pp*R_K minus *pp*R (a), *pp*R_M minus *pp*R (b), and *pp*R_O minus *pp*R (c) difference FTIR spectra of SETC (—) and the wild type (•••) in the 1780–1610 cm^{-1} region, which are reproduced from Figure 2. One division of the *y*-axis corresponds to 0.016 absorbance units.

The solid line in Figure 2c shows that of SETC measured at 240 K and pH 5. Similar difference spectra in the fingerprint region (1300–1100 cm^{-1}) as well as the HOOP region (1000–900 cm^{-1}) imply similar configuration changes of retinal between SETC and the wild type. In particular, three peaks at 1203 (−), 1192 (+), and 1178 (+) cm^{-1} with similar amplitudes between the solid and dotted lines in Figure 2c strongly suggest that similar intermediate states are formed between SETC and the wild type. Thus, we regard the solid line in Figure 2c as the *pp*R_O minus *pp*R spectrum of SETC, as described from the chromophore structure. Nevertheless, a prominent spectral difference between SETC (—) and the wild type (•••) was seen in the 1800–1600 cm^{-1} region that monitors protein structural changes. This suggests that the protein structures of the O intermediate are different between SETC and the wild type, which is possibly correlated with the lifetime of *pp*R_O (*37*). Below, we analyze the spectra of this frequency region in more detail.

Infrared Spectral Changes of the SETC Mutant of ppR upon the Formation of the K, M, and O Intermediates in the 1780–1610 cm^{-1} Region. As described above, the infrared difference spectrum in this frequency region contains vibrational bands of protein. In previous papers, we showed that carbonyl stretching vibrations of Asn105 appear at 1700 (+)/1704 (−) cm^{-1}, at 1707 (+)/ 1701 (−) cm^{-1}, and at 1708 (+)/1702 (−) cm^{-1} in the *pp*R_K minus *pp*R (Figure 3a, (•••)), *pp*R_M minus *pp*R (Figure 3b, dotted line), and *pp*R_O minus *pp*R (Figure 3c, (•••)) spectra, respectively (*5, 40, 46*). These

spectral features are essentially preserved in SETC, though the bands are considerably reduced in the *p*pR$_O$ minus *p*pR (Figure 3c, (—)) spectrum. Thus, the local structure around Asn105 is similar during the photocycles of SETC and the wild type.

We also assigned the protonated carboxyl stretching vibrations of Asp75 at 1765 cm^{-1} in both *p*pR$_M$ minus *p*pR and *p*pR$_O$ minus *p*pR spectra (*5*). It should be noted that the *p*pR$_O$ minus *p*pR spectrum of the wild type shows a shoulder band at 1757 cm^{-1} regardless of the presence ((—) in Figure 3c) and absence (*40*) of NaCl, which was also reported by other groups (*47, 48*). In the *p*pR$_M$ minus *p*pR and *p*pR$_O$ minus *p*pR spectra of SETC, the frequencies of these bands are similar to those of the wild type, whereas the intensity of the bands significantly decreased in the *p*pR$_O$ minus *p*pR spectrum of SETC (Figure 3c, (—)). In particular, the negative band 1724 cm^{-1} disappeared in SETC, whose origin is currently unidentified. These observations were common in the SET mutant of *p*pR (data not shown), suggesting that the structural changes of these residues might be inhibited upon the formation of the O intermediate and might be related to O-decay acceleration.

Secondary structural alterations can be monitored by amide I vibration at 1690–1610 cm^{-1}. In the *p*pR$_K$ minus *p*pR spectrum, the 1650 (−) cm^{-1} band of the wild type disappeared in SETC, while the 1663 (−) cm^{-1} band newly appeared in SETC that is characteristic of an α_{II}-helix. The disappearance of the 1650 (−) cm^{-1} band and the appearance of the 1663 (−)-cm^{-1} band were also observed in the T204C single mutant (see Figure 5a), but not observed in the SET mutant (data not shown), implying that this structural perturbation was caused by a mutation at the Thr204 position. The FTIR spectra of M and O intermediates in the T204C single mutant were quite similar to those of the wild type (see Figure 5), and the decay-rate constants of M and O intermediates of T204C were similar to those of the wild type (*37*). Therefore, these structural changes are not correlated with the O-decay acceleration of the *p*pR mutants.

While the *p*pR$_M$ minus *p*pR spectra exhibit similar amide I vibrations between SETC and the wild type (Figure 3b), the *p*pR$_O$ minus *p*pR spectra are significantly different between them (Figure 3c). In the wild type, strong bands at 1665 (−) and 1644 (+) cm^{-1} ((•••) in Figure 3c) indicate that the *p*pR$_O$ formation accompanies structural perturbation of the α-helix, where the hydrogen bond is strengthened. Such a spectral feature is entirely different in SETC. In SETC, the bands at 1673 (+)/1656 (−) cm^{-1} newly appeared in the frequency region typical for the amide I vibration of the α_{II}- and α_I-helices, respectively. It should be noted that such a spectral feature was observed for SET (data not shown), but not for T204C (see Figure 5), suggesting that the helical perturbation in *p*pR$_O$ originates from the amino acids at the extracellular surface.

Correlation between the Band Intensities at 1673 cm^{-1} and the O-Decay Half-Time. Are these structural changes of α-helices correlated with an acceleration of O-decay? We previously found that besides the SETC mutant, some mutants, P183E, T204C, and SET, accelerated O-decay (*37*). Therefore, we measured the *p*pR$_O$ minus *p*pR spectra of these mutants and analyzed the bands at 1673 (+)/1656 (−) cm^{-1} as shown in the inset of Figure 4. Open circles in the upper

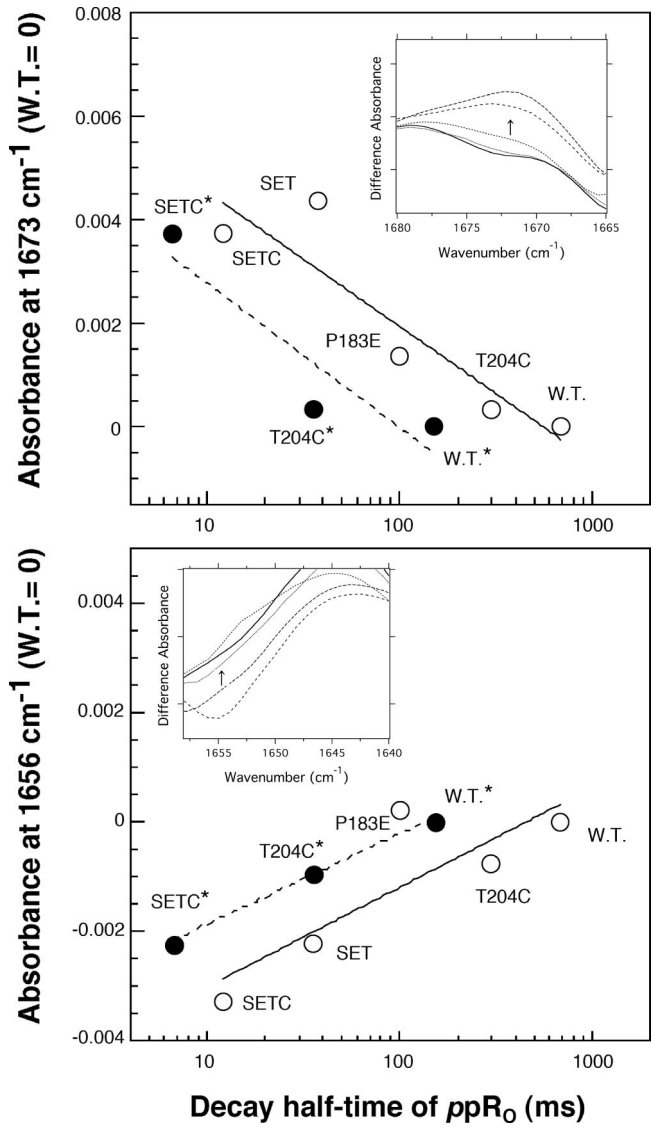

FIGURE 4: Relationship between absorbances at 1673 (upper panel) and 1656 (lower panel) cm^{-1} in the *p*pR$_O$ minus *p*pR spectra and the O-decay half-time (○). The closed circles (●) show the relationship between the absorbances and the O-decay half-time in the presence of azide. The O-decay half-times are from ref *37*. Solid and dotted lines are fitting curves. The inset shows the *p*pR$_O$ minus *p*pR difference FTIR spectra of the wild type and various O-decay accelerated mutants in each frequency region (spectra for wild type, T204C, P183E, SETC, and SET from the bottom to top at 1673 cm^{-1}, and for SETC, SET, T204C, P183E, and wild type from the bottom to top at 1656 cm^{-1}). One division of the *y*-axis corresponds to 0.004 absorbance units.

panel of Figure 4 plot the intensities of the bands at 1673 cm^{-1} versus O-decay half-times in the literature (*37*). In the cases of T204C and SETC, we could not directly determine the O-decay half-time because of the slow decay of the preceding *p*pR$_M$ (*37*). Therefore, we predicted the half-time from the pK_a values of Asp75 because the decay half-times were well correlated with the pK_a value of Asp75 as reported previously (*37*). In addition, we used O-decay half-times in the presence of azide (●) (*37*), which selectively accelerates M-decay (*49*). Consequently, the O-decay half-times are positively correlated with the enhanced intensities of the bands at 1673 cm^{-1} ((—) and (•••) in Figure 4). Such a positive correlation shows that the structural changes in *p*pR$_O$ are crucial for the acceleration in O-decay.

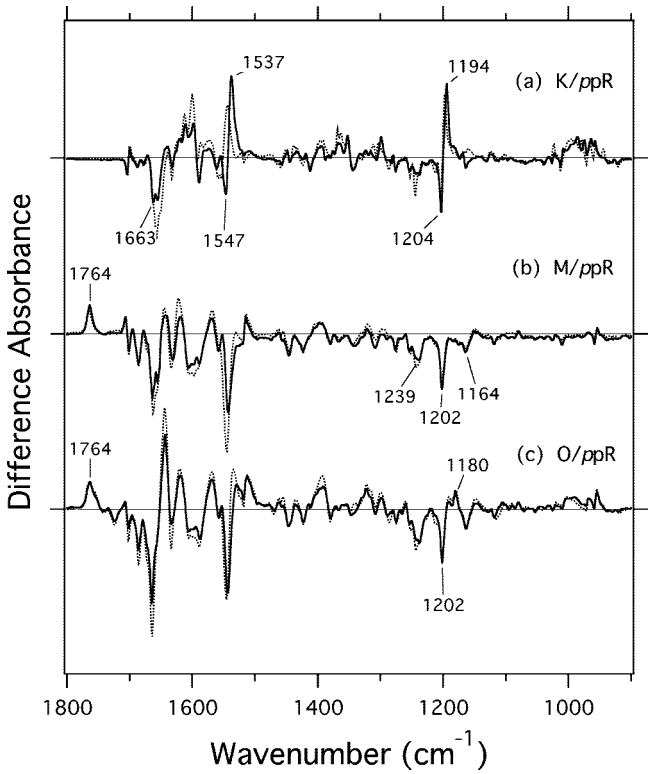

FIGURE 5: $pp\mathrm{R_K}$ minus *pp*R (a), $pp\mathrm{R_M}$ minus *pp*R (b), and $pp\mathrm{R_O}$ minus *pp*R (c) difference FTIR spectra of T204C (—) and the wild type (•••) in the 1800–900 cm^{-1} region. These spectra of T204C were measured at 77 K and pH 7 (a), 230 K and pH 7 (b), and 260 K and pH 5 (c). One division of the *y*-axis corresponds to 0.013 absorbance units.

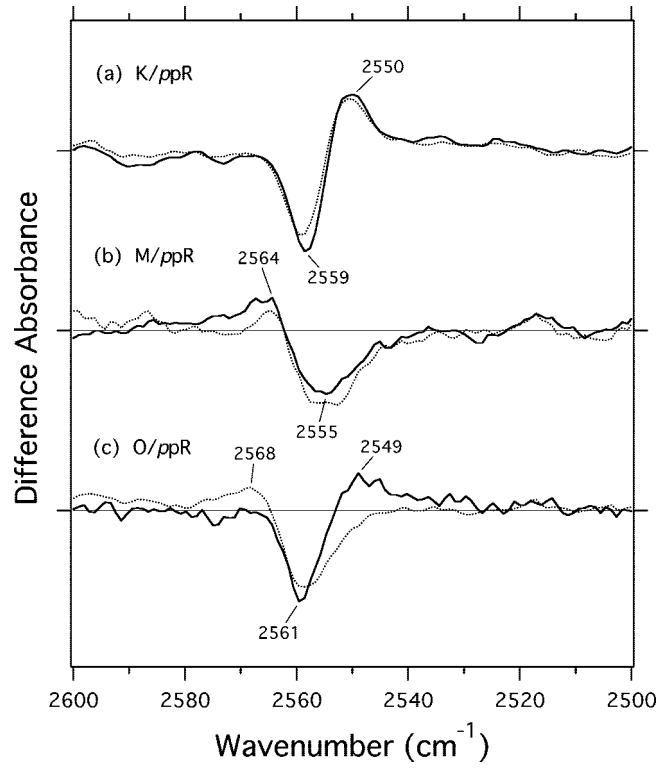

FIGURE 6: $pp\mathrm{R_K}$ minus *pp*R (a), $pp\mathrm{R_M}$ minus *pp*R (b), and $pp\mathrm{R_O}$ minus *pp*R (c) difference FTIR spectra of T204C (•••) and SETC (—) in the 2600–2500 cm^{-1} region. One division of the *y*-axis corresponds to 0.0007 absorbance units. The $pp\mathrm{R_M}$ minus *pp*R and $pp\mathrm{R_O}$ minus *pp*R difference FTIR spectra are increased by a factor of 2.5 and 2, respectively, for the sake of comparison.

The lower panel of Figure 4 shows similar analysis for the negative band at 1656 cm^{-1}. It should be noted that this frequency region contains many vibrational bands such as the amide I vibration of the α_I-helix and the C=N stretching vibration of the retinal Schiff base. Nevertheless, a similar positive correlation was obtained.

Infrared Spectral Changes of the SETC Mutant of ppR upon the Formation of the K, M, and O Intermediates in the S−H Stretching Frequency Region (2580–2525 cm^{-1}). Frequencies of the cysteine S−H stretches are well isolated from other vibrations (*50*). This is advantageous for analyzing their hydrogen-bonding conditions as has been shown for the LOV domains of phototropin (*51, 52*). It is further useful for the analysis of the engineered BR (*50*) and SRII (*53*), where an alteration in the hydrogen bonding of specific amino acids was mimicked by introducing a cysteine. Similarly, we can monitor the S−H stretching vibration in the O-decay accelerated mutant (SETC) because this mutant has only one cystein residue (Cys204).

Figure 5 compares the $pp\mathrm{R_K}$ minus *pp*R, $pp\mathrm{R_M}$ minus *pp*R, and $pp\mathrm{R_O}$ minus *pp*R difference infrared spectra between T204C (—) and the wild type (•••). The 1547 (−)/1537 (+), 1204 (−)/1194 (+), 1239 (−), 1202 (−), 1164 (−), and 1202 (−)/1180 (+) cm^{-1} bands in T204C originate from the retinal chromophore in Figure 5a, b, and c, which are very similar to those of the wild type. The protonated carboxyl stretching vibration bands of Asp75 at 1765 cm^{-1} in both the $pp\mathrm{R_M}$ minus *pp*R and $pp\mathrm{R_O}$ minus *pp*R spectra and the amide I vibration bands were also very similar to those of the wild type, implying protein structural changes similar to those of the wild type during the photocycle in the T204C mutant. Furthermore, we previously confirmed that the T204C mutant of *pp*R mediated normal phototaxis like the wild type (*53*). Thus, the T204C mutant retains the structural changes of the wild type and is useful for the analysis of protein conformational changes and hydrogen bonding alteration of the S−H stretching vibration of Cys204 (*53*).

Figure 6 shows infrared spectral changes of the SETC (—) and T204C (•••) of *pp*R upon formation of the K, M, and O intermediates in the S−H stretching frequency region. The S−H vibration bands in SETC appeared at 2559 (−)/2550 (+) cm^{-1} for the $pp\mathrm{R_K}$ minus *pp*R and 2555 (−)/2564 (+) cm^{-1} for the $pp\mathrm{R_M}$ minus *pp*R spectra. In the $pp\mathrm{R_K}$ minus *pp*R (Figure 6a) and the $pp\mathrm{R_M}$ minus *pp*R spectra (Figure 6b), both the dotted and solid lines look similar in this frequency region, indicating similar structural changes of Cys204 upon the formation of K and M intermediates. In contrast, the dotted and solid lines in Figure 6c are clearly different. The O intermediates of T204C and SETC possess the S−H stretch of Cys204 at 2568 (•••) and 2549 (—) cm^{-1}, respectively. It should be noted that the hydrogen-bonding conditions of Cys204 are affected by mutations at the extracellular surface. These characteristic changes of the S−H group of Cys204 are probably related to the acceleration in O-decay. Interestingly, the upshift of the S−H stretching vibration of Cys204 is also observed for the spectrum in the presence of *p*HtrII (*53*).

DISCUSSION

In the present study, we studied structural alterations of the O-decay accelerating mutants of *pp*R by means of low-

temperature FTIR spectroscopy. The C=C and C−C stretching vibrations of the retinal chromophore were similar between the wild type and SETC for the unphotolyzed, K, M, and O intermediate states (Figure 2). Light-minus-dark FTIR spectra were further similar for the K and M states. In contrast, protein structural alterations in the O state were highly different between the wild type and SETC. The most prominent spectral feature of SETC was the absence of the amide I vibration of the wild type at 1665 (−)/1644 (+) cm^{-1} and the concomitant appearance of the amide I vibration at 1673 (+)/1656 (−) cm^{-1} (Figure 3c). In various O-decay accelerating mutants, the absorbances of the bands at 1673 (+)/1656 (−) cm^{-1} were well correlated with the O-decay half-time (Figure 4). The frequencies are characteristic for the amide-I vibrations of the α_{II}- and α_{I}-helices. Since the α_{II}-helix possesses a considerably distorted structure, helix distortion is probably required for accelerating O-decay in *p*pR.

Then, how do such structural changes occur? *p*pR has a relatively hydrophobic proton conduction channel at the extracellular (EC) side compared to that of BR, where Ser193, Glu194, and Thr205 in BR are replaced by the hydrophobic residues Pro182, Pro183, and Val194, respectively (Figure 1) (*36*). On the basis of knowledge about BR and the present FTIR and previous flash-photolysis data for *p*pR (*29, 37*), we inferred the following mechanism. A hydrogen-bonding network on the EC side plays an important role for O-decay in BR where polar residues must take part in proton transfer from Asp85 to the proton release group (PRG). In the case of *p*pR, a proton pump occurs in the absence of the transducer protein, but the efficiency is lower than that in BR (*24, 25*). Thus, the proton attached to Asp75 is transferred to the EC aqueous phase through a limited hydrogen-bonding network (proton pump) or to the retinal Schiff base (no pump) during the O-decay of the wild-type *p*pR. In SETC, a newly formed hydrogen-bonding network must help the proton transfer in the EC region, leading to the fast decay of O. Helical perturbation is presumably a prerequisite for such proton conduction. This is supported by the observation that mutation at PRG leads to a slower O-decay in BR (*33, 34*), though the O intermediate of BR does not possesses a band at 1673 cm^{-1} (*54*). On the EC channel, we reported that Arg72 formed a hydrogen bond with Asp193 (*55*), which is a putative proton-releasing residue (*56*). The O-decay process is probably regulated by such a hydrogen-bonding network.

Another noteworthy issue is the 2561 (−) cm^{-1} band in the $p pR_O$ minus *p*pR spectra of SETC and T204C, which is upshifted to 2568 cm^{-1} for T204C but downshifted to 2549 (+) cm^{-1} for SETC. The FTIR spectra were almost identical between the wild type and T204C (Figure 5). Therefore, the replacement of Pro182, Pro183, and Val184 is responsible for the downshift of the S−H stretch in SETC. This clearly shows the existence of a long-range interaction between the EC surface and the Schiff base, which is important for the acceleration of O-decay. The frequencies at 2568 and 2549 cm^{-1} correspond to weak and moderate hydrogen bonding, respectively. The X-ray crystallographic structure and previous reports suggest the existence of a hydrogen bond between Thr204 and Tyr174 (Figure 1) (*13–15, 43*), which is crucial for phototaxis function (*53*). Thus, our measurements of the S−H stretching frequency region probably monitored the hydrogen bond between Cys204 and Tyr174. If this is the case, the hydrogen bond between Cys204 and Tyr174 becomes weak upon the formation of the O intermediate in T204C (slow O-decay), whereas it becomes strong in SETC (fast O-decay). These structural changes may be a key factor to keep slow O-decay in *p*pR and fast O-decay in pumping rhodopsins, BR and hR. It is believed that the long-lived M and O intermediates are important for signal transduction to cognate transducer protein, *p*HtrII, because these intermediates occur in the signaling state (*21*), whereas the life-times of the M and O intermediates of BR and O intermediate of hR, which are ion-pumping proteins, are much shorter than photosensors, sR and *p*pR (*19*), because they are indispensable to efficient pumps. Does the acceleration of O-decay influence signal transduction and pumping activity? This is our next focus.

In conclusion, we found characteristic bands at 1673 (+)/1656 (−) cm^{-1} in the O-decay accelerated mutants. The absorbance of the bands was well correlated with the O-decay half-time. This suggests that helical distortion is important for the acceleration in O-decay. In addition, we demonstrated that characteristic changes in the S−H stretching vibration of Cys204 was observed in SETC, suggesting that structural perturbation near the Schiff base was caused by an acceleration in O-decay on the extracellular surface. Thus, FTIR analysis of the O-accelerated mutants provided us with information about the mechanism of the slow O-decay in *p*pR. The effect on phototaxis and proton pumping of *p*pR is an important question that should be examined because the O intermediate is one of the active intermediates for signal transduction and one of the important intermediates for ion pumping.

ACKNOWLEDGMENT

We thank Dr. Mikihiro Shibata for invaluable discussions.

REFERENCES

1. Klare, J. P., Gordeliy, V. I., Labahn, J., Buldt, G., Steinhoff, H. J., and Engelhard, M. (2004) The archaeal sensory rhodopsin II/transducer complex: a model for transmembrane signal transfer. *FEBS Lett. 564*, 219–224.
2. Sudo, Y., Kandori, H., and Kamo, N. (2004) Molecular mechanism of protein-protein interaction of *pharaonis* phoborhodopsin/transducer and photo-signal transfer reaction by the complex. *Recent Res. Dev. Biophys. 3*, 1–16.
3. Spudich, J. L. (2006) The multitalented microbial sensory rhodopsins. *Trends Microbiol. 14*, 480–487.
4. Engelhard, M., Scharf, B., and Siebert, F. (1996) Protonation changes during the photocycle of sensory rhodopsin II from *Natronobacterium pharaonis*. *FEBS Lett. 395*, 195–198.
5. Furutani, Y., Iwamoto, M., Shimono, K., Kamo, N., and Kandori, H. (2002) FTIR spectroscopy of the M-photointermediate in *pharaonis* phoborhodopsin. *Biophys. J. 83*, 3482–3489.
6. Haupts, U., Tittor, J., and Oesterhelt, D. (1999) Closing in on bacteriorhodopsin: progress in understanding the molecule. *Annu. Rev. Biophys. Biomol. Struct. 28*, 367–399.
7. Kandori, H. (2004) Hydration switch model for the proton transfer in the Schiff base region of bacteriorhodopsin. *Biochim. Biophys. Acta 1658*, 72–79.
8. Essen, L. O. (2002) Halorhodopsin: light-driven ion pumping made simple. *Curr. Opin. Struct. Biol. 12*, 516–522.
9. Hoff, W. D., Jung, K. H., and Spudich, J. L. (1997) Molecular mechanism of photosignaling by archaeal sensory rhodopsins. *Annu. Rev. Biophys. Biomol. Struct. 26*, 223–258.
10. Sudo, Y., Yamabi, M., Iwamoto, M., Shimono, K., and Kamo, N. (2003) Interaction of *Natronobacterium pharaonis* phoborhodopsin

(sensory rhodopsin II) with its cognate transducer probed by increase in the thermal stability. *Photochem. Photobiol. 78*, 511–516.
11. Shimono, K., Iwamoto, M., Sumi, M., and Kamo, N. (1997) Functional expression of *pharaonis* phoborhodopsin in *Escherichia coli*. *FEBS Lett. 420*, 54–56.
12. Sudo, Y., Iwamoto, M., Shimono, K., and Kamo, N. (2001) *pharaonis* phoborhodopsin binds to its cognate truncated transducer even in the presence of a detergent with a 1:1 stoichiometry. *Photochem. Photobiol. 74*, 489–494.
13. Luecke, H., Schobert, B., Lanyi, J. K., Spudich, E. N., and Spudich, J. L. (2001) Crystal structure of sensory rhodopsin II at 2.4 angstroms: insights into color tuning and transducer interaction. *Science 293*, 1499–1503.
14. Royant, A., Nollert, P., Edman, K., Neutze, R., Landau, E. M., Pebay-Peyroula, E., and Navarro, J. (2001) X-ray structure of sensory rhodopsin II at 2.1-Å resolution. *Proc. Natl. Acad. Sci. U.S.A. 98*, 10131–10136.
15. Gordeliy, V. I., Labahn, J., Moukhametzianov, R., Efremov, R., Granzin, J., Schlesinger, R., Buldt, G., Savopol, T., Scheidig, A. J., Klare, J. P., and Engelhard, M. (2002) Molecular basis of transmembrane signalling by sensory rhodopsin II-transducer complex. *Nature 419*, 484–487.
16. Luecke, H., Schobert, B., Richter, H.-T., Cartailler, J. P., and Lanyi, J. K. (1999) Structure of bacteriorhodopsin at 1.55 Å resolution. *J. Mol. Biol. 291*, 899–911.
17. Sudo, Y., and Spudich, J. L. (2006) Three strategically placed hydrogen-bonding residues convert a proton pump into a sensory receptor. *Proc. Natl. Acad. Sci. U.S.A. 103*, 16129–16134.
18. Sudo, Y., Furutani, Y., Spudich, J. L., and Kandori, H. (2007) Early photocycle structural changes in a bacteriorhodopsin mutant engineered to transmit photosensory signals. *J. Biol. Chem. 282*, 15550–15558.
19. Iwamoto, M., Kandori, H., and Kamo, N. (2003) Photochemical properties of *pharaonis* phoborhodopsin (sensory rhodopsin II). *Recent Res. Dev. Chem. 1*, 15–30.
20. Chizhov, I., Schmies, G., Seidel, R., Sydor, J. R., Luttenberg, B., and Engelhard, M. (1998) The photophobic receptor from *Natronobacterium pharaonis*: temperature and pH dependencies of the photocycle of sensory rhodopsin II. *Biophys. J. 75*, 999–1009.
21. Yan, B., Takahashi, T., Johnson, R., and Spudich, J. L. (1991) Identification of signaling states of a sensory receptor by modulation of lifetimes of stimulus-induced conformations: the case of sensory rhodopsin II. *Biochemistry 30*, 10686–10692.
22. Braiman, M. S., Bousche, O., and Rothschild, K. J. (1991) Protein dynamics in the bacteriorhodopsin photocycle: submillisecond Fourier transform infrared spectra of the L, M, and N photointermediates. *Proc. Natl. Acad. Sci. U.S.A. 88*, 2388–2392.
23. Brown, L. S., and Lanyi, J. K. (1996) Determination of the transiently lowered pKa of the retinal Schiff base during the photocycle of bacteriorhodopsin. *Proc. Natl. Acad. Sci. U.S.A. 93*, 1731–1734.
24. Schmies, G., Luttenberg, B., Chizhov, I., Engelhard, M., Becker, A., and Bamberg, E. (2000) Sensory rhodopsin II from the haloalkaliphilic *Natronobacterium pharaonis*: light-activated proton transfer reactions. *Biophys. J. 78*, 967–976.
25. Sudo, Y., Iwamoto, M., Shimono, K., Sumi, M., and Kamo, N. (2001) Photo-induced proton transport of *pharaonis* phoborhodopsin (sensory rhodopsin II) is ceased by association with the transducer. *Biophys. J. 80*, 916–922.
26. Holz, M., Drachev, L. A., Mogi, T., Otto, H., Kaulen, A. D., Heyn, M. P., Skulachev, V. P., and Khorana, H. G. (1989) Replacement of aspartic acid-96 by asparagine in bacteriorhodopsin slows both the decay of the M intermediate and the associated proton movement. *Proc. Natl. Acad. Sci. U.S.A. 86*, 2167–2171.
27. Marti, T., Otto, H., Mogi, T., Rosselet, S. J., Heyn, M. P., and Khorana, H. G. (1991) Bacteriorhodopsin mutants containing single substitutions of serine or threonine residues are all active in proton translocation. *J. Biol. Chem. 266*, 6919–6927.
28. Iwamoto, M., Shimono, K., Sumi, M., and Kamo, N. (1999) Positioning proton-donating residues to the Schiff-base accelerates the M-decay of *pharaonis* phoborhodopsin expressed in *Escherichia coli*. *Biophys. Chem. 79*, 187–192.
29. Iwamoto, M., Furutani, Y., Kamo, N., and Kandori, H. (2003) Proton transfer reactions in the F86D and F86E mutants of pharaonis *phoborhodopsin* (sensory rhodopsin II). *Biochemistry 42*, 2790–2796.
30. Yoshida, H., Sudo, Y., Shimono, K., Iwamoto, M., and Kamo, N. (2004) Transient movement of helix F revealed by photo-induced inactivation by reaction of a bulky SH-reagent to cycteine-introduced *pharaonis* phoborhodopsin (sensory rhodopsin II). *Photochem. Photobiol. Sci. 3*, 537–542.
31. Brown, L. S., Sasaki, J., Kandori, H., Maeda, A., Needleman, R., and Lanyi, J. K. (1995) Glutamic acid 204 is the terminal proton release group at the extracellular surface of bacteriorhodopsin. *J. Biol. Chem. 270*, 27122–27126.
32. Richter, H. T., Brown, L. S., Needleman, R., and Lanyi, J. K. (1996) A linkage of the pKa's of Asp-85 and Glu-204 forms part of the reprotonation switch of bacteriorhodopsin. *Biochemistry 35*, 4054–4062.
33. Balashov, S. P., Imasheva, E. S., Ebrey, T. G., Chen, B. N., Menick, D. R., and Crouch, R. K. (1997) Glutamate-194 to cysteine mutation inhibits fast light-induced proton release in bacteriorhodopsin. *Biochemistry 36*, 8671–8676.
34. Balashov, S. P., Lu, M., Imasheva, E. S., Govindjee, R., Ebrey, T. G., Othersen, B., III, Chen, Y., Crouch, R. K., and Menick, D. R. (1999) The proton release group of bacteriorhodopsin controls the rate of the final step of its photocycle at low pH. *Biochemistry 38*, 2026–2039.
35. Dioumaev, A. K., Brown, L. S., Needleman, R., and Lanyi, J. K. (1999) Fourier transform infrared spectra of a late intermediate of the bacteriorhodopsin photocycle suggest transient protonation of Asp-212. *Biochemistry 38*, 10070–10078.
36. Seidel, R., Scharf, B., Gautel, M., Kleine, K., Oesterhelt, D., and Engelhard, M. (1995) The primary structure of sensory rhodopsin II: a member of an additional retinal protein subgroup is coexpressed with its transducer, the halobacterial transducer of rhodopsin II. *Proc. Natl. Acad. Sci. U.S.A. 92*, 3036–3040.
37. Iwamoto, M., Sudo, Y., Shimono, K., Araiso, T., and Kamo, N. (2005) Correlation of the O-intermediate rate with the pKa of Asp75 in the dark, the counterion of the Schiff base of *pharaonis* phoborhodopsin (sensory rhodopsin II). *Biophys. J. 88*, 1215–1223.
38. Furutani, Y., and Kandori, H. (2002) Internal water molecules of archaeal rhodopsins. *Mol. Membr. Biol. 19*, 257–265.
39. Kandori, H., Shimono, K., Sudo, Y., Iwamoto, M., Shichida, Y., and Kamo, N. (2001) Structural changes of pharaonis *phoborhodopsin* upon photoisomerization of the retinal chromophore: Infrared spectral comparison with bacteriorhodopsin. *Biochemistry 40*, 9238–9246.
40. Furutani, Y., Iwamoto, M., Shimono, K., Wada, A., Ito, M., Kamo, N., and Kandori, H. (2004) FTIR spectroscopy of the O photointermediate in pharaonis *phoborhodopsin*. *Biochemistry 43*, 5204–5212.
41. Shimono, K., Hayashi, T., Ikeura, Y., Sudo, Y., Iwamoto, M., and Kamo, N. (2003) Importance of the broad regional interaction for spectral tuning in *Natronobacterium pharaonis* phoborhodopsin (sensory rhodopsin II). *J. Biol. Chem. 278*, 23882–23889.
42. Klare, J. P., Schmies, G., Chizhov, I., Shimono, K., Kamo, N., and Engelhard, M. (2002) Probing the proton channel and the retinal binding site of *Natronobacterium pharaonis* sensory rhodopsin II. *Biophys. J. 82*, 2156–2164.
43. Sudo, Y., Furutani, Y., Shimono, K., Kamo, N., and Kandori, H. (2003) Hydrogen bonding alteration of Thr-204 in the complex between *pharaonis* phoborhodopsin and its transducer protein. *Biochemistry 42*, 14166–14172.
44. Zscherp, C., and Heberle, J. (1997) Infrared difference spectra of the intermediates L, M, N, and O of the bacteriorhodopsin photoreaction obtained by time-resolved attenuated total reflection spectroscopy. *J. Phys. Chem. B 101*, 10542–10547.
45. Smith, S. O., Pardoen, J. A., Mulder, P. P. J., Curry, B., Lugtenburg, J., and Mathies, R. A. (1983) Chromophore structure in bacteriorhodopsin's O640 photointermedaite. *Biochemistry 22*, 6141–6148.
46. Kandori, H., Shimono, K., Shichida, Y., and Kamo, N. (2002) Interaction of Asn105 with the retinal chromophore during photoisomerization of pharaonis *phoborhodopsin*. *Biochemistry 41*, 4554–4559.
47. Hein, M., Wegener, A. A., Engelhard, M., and Siebert, F. (2003) Time-resolved FTIR studies of sensory rhodopsin II (NpSRII) from *Natronobacterium pharaonis*: implications for proton transport and receptor activation. *Biophys. J. 84*, 1208–1217.
48. Bergo, V., Spudich, E. N., Spudich, J. L., and Rothschild, K. J. (2003) Conformational changes detected in a sensory rhodopsin II-transducer complex. *J. Biol. Chem. 278*, 36556–36562.
49. Iwamoto, M., Sudo, Y., Shimono, K., and Kamo, N. (2001) Selective reaction of hydroxylamine with chromophore during the photocycle of pharaonis *phoborhodopsin*. *Biochim. Biophys. Acta 1514*, 152–158.

50. Kandori, H., Kinoshita, N., Shichida, Y., Maeda, A., Needleman, R., and Lanyi, J. K. (1998) Cysteine S-H as a hydrogen-bonding probe in proteins. *J. Am. Chem. Soc. 120*, 5828–5829.
51. Iwata, T., Tokutomi, S., and Kandori, H. (2002) Photoreaction of the cysteine S-H group in the LOV2 domain of *Adiantum* phytochrome3. *J. Am. Chem. Soc. 124*, 11840–11841.
52. Sato, Y., Iwata, T., Tokutomi, S., and Kandori, H. (2005) Reactive cysteine is protonated in the triplet excited state of the LOV2 domain in *Adiantum* phytochrome3. *J. Am. Chem. Soc. 127*, 1088–1089.
53. Sudo, Y., Furutani, Y., Kandori, H., and Spudich, J. L. (2006) Functional importance of the interhelical hydrogen bond between Thr204 and Tyr174 of sensory rhodopsin II and its alteration during the signaling process. *J. Biol. Chem. 281*, 34239–34245.
54. Hessling, B., Souvignier, G., and Gerwert, K. (1993) A model-independent approach to assigning bacteriorhodopsin's intramolecular reactions to photocycle intermediates. *Biophys. J. 65*, 1929–1941.
55. Ikeura, Y., Shimono, K., Iwamoto, M., Sudo, Y., and Kamo, N. (2004) Role of Arg-72 of *pharaonis* phoborhodopsin (sensory rhodopsin II) on its photochemistry. *Biophys. J. 86*, 3112–3120.
56. Iwamoto, M., Hasegawa, C., Sudo, Y., Shimono, K., Araiso, T., and Kamo, N. (2004) Proton release and uptake of pharaonis *phoborhodopsin* (sensory rhodopsin II) reconstituted into phospholipids. *Biochemistry 43*, 3195–3203.

BI701885K